CrossMark

ORIGINAL PAPER

Reactive compatibilization of polyetherimide with polyamide 6,6: part 1. Effect of functionalizing polyetherimide

Yeh Wang[1] · **Chih-Min Chien**[2] · **Shu-Min Chiao**[1] · **Tzan-Yu Lee**[1]

Abstract   The functionalized polyetherimides (fPEIs) grafted with maleic anhydride (MA) or glycidyl methacrylate (GMA) was synthesized through reactive melt blending. The compatibility and interaction of polyamide 6,6 (PA66) and fPEI in the blends were characterized by Fourier transform infrared spectra, Molau tests, melt flow index, dynamic mechanical analysis, thermal mechanical analysis, and scanning electron microscopy. Izod impact strength and heat deflection temperature tests were performed to determine thermal and mechanical properties. The results show that fPEIs can react with the amino end groups in PA66. In this way, the in situ-formed fPEI-*g*-PA66 copolymer compatibilizer anchors at the interface of PA66/fPEI blends. The morphological study of the fracture sections before and after impact test revealed that the fPEI particles were dispersed uniformly in the PA66 matrix and the interfacial adhesion between PA66 and fPEI was increased significantly. The mechanical properties of the modified blends were enhanced compared with the unmodified PA66/PEI pair due to the improvement in the compatibility between the individual components.

Introduction

Polymer blends offer enormous potential in polymer modification because they allow for simple processing and unlimited possibilities in designing novel materials that combine advantageous properties of different polymers [1, 2]. Due to intense commercial interest in materials with specifically tailored end-use properties, polymer blending has become a major issue in the field of polymer science and

✉ Yeh Wang
yehwang@thu.edu.tw

[1]   Tunghai University, Taichung, Taiwan

[2]   Taiwan Textile Research Institute, New Taipei, Taiwan

technology during the last three decades. Currently, polymer blends constitute more than 10 wt% of the total polymer consumption, and their economic significance continues to increase [3].

Polyamide (PA), also known as nylon, is one of the most versatile engineering plastics. PA66 is an important engineering plastic in the PA family due to its excellent performance, large-scale production and wide application [4]. Because of its excellent balance of strength, ductility and stiffness, exceptional chemical and solvent resistance, and ease of fabrication and processing [5–7], PA66 is widely applied in areas such as automobile, electronics, machinery, packaging, sports, consumer goods, and so on [8, 9]. However, it is well known that PA66 is prone to absorb moisture due to the backbone polar amide groups [10], and at low temperature has high sensitivity to notch propagation under impact, which easily leads to embrittlement [11]. In addition, its inferior electrical properties compared to polyethylene or polypropylene, its relatively lower dimensional stability and heat resistance compared with most other engineering plastics, limit the wider application of PA66 [12]. Therefore, in recent years [13–16], more attention has been paid to the modifications of PA66 to develop new products with outstanding properties to broaden its applications in electronic and automotive industries. Indeed blending PA66 with various high-performance polymers [12, 16–19] offers an efficient and economic alternative despite recent progress in synthesis of high-temperature nylons with aromatic backbones such as polyterephthalamides and polyamide-imide [20, 21].

On the other hand, polyetherimide (PEI), an amorphous polymer commercially known as Ultem, has favorable high-performance properties [22–24], and is characterized by a high glass transition temperature (T_g) of around 220 °C. The ether units lend the structure flexible linkages. The aromatic imide units provide high heat resistance, dimensional stability and good mechanical properties. Furthermore, the high proportion of aromatic rings gives this polymer excellent thermal stability and flame retardancy, but like many other high-performing thermoplastic materials PEI has low stress crack resistance and high melt viscosities [25]. Therefore, blending PEI with partially crystalline polymers like polyamides, which have excellent stress crack resistance and good flow properties, could be an appropriate way to create new materials with tailor-made properties. PEI has been blended with various engineering polymers [26–28] to form partially miscible blends with improved processability. However, the development of PA66 and PEI blends is rather lagging behind.

The aim of the present study is to introduce PEI containing rigid segments to PA66, in order to improve performance and to explore the relationship between the microstructure and the properties of the novel in situ blends. To the best of our knowledge, few studies to date concerning these aspects have been reported [12, 29–33]. In addition, the difference in compatibilization behavior between the in situ-formed copolymers during melt blending will be examined. We shall carry out melt blending of functionalized PEI with PA66 at 40/60 weight ratio using a miniature mixer. Two types of functionalized PEIs (fPEIs) with different degree of grafting are used, i.e., maleic anhydride (MA) and glycidyl methacrylate (GMA)-grafted PEI (PEIgMA and PEIgGMA). The morphology developments are studied by scanning

electron microscopy (SEM). The stability of in situ-formed copolymer at the interface was investigated at quiescent condition and the result was compared with that at dynamic condition through morphological observation. The in situ copolymer formation was further confirmed by FTIR and the Molau test. The DMA results indicate that functionalized PEIs can also form entanglement with PA66 matrix. In this way, the in situ-formed PEI-*g*-PA66 anchors at the interface and leads to the suppression of PEI particle aggregation and enhancement of interfacial adhesion. The mechanical properties are consequently improved.

Experimental

Materials

The polymers used in this work were of commercial grade nylon 6,6 (PA66) of DuPont, Zytel® 101L; and polyetherimide (PEI) of SABIC, Ultem™ HU1010. The thermal, mechanical and flow properties of the base polymers are listed in Table 1. Two fPEIs, PEIgMAs and PEIgGMAs, of different degree of grafting (DG) were used as reactive components. Both GMA and MA are reagent grades of Showa Chemicals Japan with purity over 95 %; and the radical initiator dicumyl peroxide (DCP) is also a reagent grade of Acros with purity over 99 %. The PA stabilizer, tris (2,4-di-tert-butylphenyl) phosphate (Everfos® 168) is a commercial grade of Everspring Chemical Co. Taiwan with purity over 99 %. The solvent for PEI, *N*-methyl-2-pyrrolidone (NMP), is an HPLC grade of Chang Chun Petrochemical Co. Taiwan with purity over 99.5 %. All the chemical regents were used as received.

Synthesis of functionalized PEI

The functionalization of PEI is similar to the grafting of polyethersulfone [34]. PEI pellet was dried under vacuum for 4 h at 150 °C to ensure removal of any absorbed moisture. Next, PEI, MA or GMA, and DCP were physically premixed. The recipe consisted of 50 g PEI, and 5 and 10 phr of MA or GMA. The amount of DCP was 0.5 phr based on the weight basis of PEI. The reactive grafting process was carried out in a roller mixer (Brabender plastograph EC, Germany) at 300 °C and 100 rpm

Table 1 Thermal and mechanical properties of neat resins

	T_d (°C)	T_m (°C)	T_g (°C)	T_s (°C)	HDT (°C)	MFI g/10 min	IS (J/m)
PEI	544	–	223	220	209	5.53	48.6 ± 2.0
PA66	460	265.7	76	76	248	270	51.8 ± 2.3

T_d degradation temperature by TGA, T_m melting temperature by DSC, T_g glass transition temperature by DMA, T_s softening temperature by TMAm, T_s softening temperature by TMA, *HDT* heat deflection temperature by ASTM D648, *MFI* melt flow index by ASTM D1238 at 300 °C, *IS* notched Izod impact strength by ASTM D256

for 5 min when both the torque and the temperature became steady. After grafting, purification process was carried out. PEIgMA or GMA was agitated in NMP at 60 °C for 2 h, and the hot solution was poured into cold acetone. The precipitated polymer was washed with acetone several times, to remove any unreacted reagents, followed by drying in a vacuum oven at 80 °C for 24 h. The purified functionalized PEI (fPEI) was stored in sealed bag with desiccant for later use. The FTIR analysis and the grafting reactions between PEI and the reacting monomers will be discussed later.

Titration and degree of grafting of PEIgGMA and PEIgMA

A brief description of the epoxide titration is given here. The detailed procedures can be found elsewhere [35]. A certain amount of samples with 10 mL hydrochloric acid–acetone solution were loaded into a conical flask with a ground glass stopper. After ultrasonication and dissolution of the samples, 3–5 drops of a phenolphthalein indicator were added into the flask and the solution was titrated with a KOH/EtOH solution to a pink color which did not fade within 10 s. Each set of data was measured three times and the average values were taken as the end results.

Back titrations are used to determine epoxide values of grafted GMA; the excess hydrochloric acid is titrated with NaOH after the addition reaction of the epoxide group with HCl. The degree of grafting (DG) of GMA was calculated by the following formula:

$$DG(GMA) = N * (V_o - V) * 143.15/(W * 1000) * 100 \%, \tag{1}$$

where V and V_o are the volumes (mL) of the NaOH standard aqueous solution consumed by the hydrochloric acid–acetone solution with and without dissolved samples, respectively. N (mol/L) is the normal concentration of the KOH/EtOH solution, and W is the mass (g) of the sample.

Degree of grafting for PEIgMA was also determined through titration [36]. A certain amount of purified PEIgMA was refluxed in 100 mL of NMP for 1 h. It was then titrated immediately with 0.005 N potassium hydroxide in ethanol (KOH/EtOH), using phenolphthalein as indicator. The DG can be calculated by:

$$DG(MA) = N * (V - V_o) * 98.06/(2 * W * 1000) * 100 \%, \tag{2}$$

where N (mol/L) is the normal concentration of NaOH/EtOH solution, W is the sample weight (g), V_o and V are the KOH/EtOH volumes (mL) for blank solution and for titration of PEIgMA, respectively. All characteristic data of fPEIs are summarized in Table 2. Note that PEIgGMAs with feed ratios of 5 and 10 phr GMA are abbreviated as PG5 and PG10, respectively. Similarly, PM5 and PM10 denoted PEIgMAs with 5 and 10 phr MA feed. The DG (Eq. 1) of PG5 and PG10 are 1.9 % ± 0.12 and 2.3 % ± 0.08, respectively; and the DG (Eq. 2) of PM5 and PM10 are 2.4 % ± 0.13 and 3.5 % ± 0.17, respectively. The mechanical and thermal properties of fPEI were generally lower than that of the virgin PEI (see Table 1) except that the MFIs of fPEIs were lower due to polar interaction among the grafted functional groups.

Table 2 Thermal and mechanical properties of fPEIs

Name code	Degree of grafting	T_d (°C)	T_g (°C)	E' (MPa) 30 °C	E' (MPa) 200 °C	T_s (°C)	HDT (°C)	MFI (g/ 10 min)	IS (J/m)
PEI	–	544	223	429	390	220	209	5.53	48.6 ± 2.02
PG5	1.9 % ± 0.12	534	219	383	355	216	213	5.19	40.3 ± 1.46
PG10	2.3 % ± 0.08	520	216	300	298	214	212	4.77	35.7 ± 1.23

T_d degradation temperature by TGA, T_g glass transition temperature by DMA, T_s softening temperature by TMA, *HDT* heat deflection temperature by ASTM D648, *MFI* melt flow index by ASTM D1238 at 300 °C, *IS* notched Izod impact strength by ASTM D256

Blend preparation

Various reacted blends of PA66/fPEI with a weight ratio of 60–40 were prepared using the following procedure. Both PA66 and purified fPEI were dried under vacuum for 4 h at 80 and 150 °C, respectively. Next, dried fPEI was transferred to the plasticorder, which was preheated to 300 °C and operated at 100 rpm until steady torque reached. Then dried PA66 pellet was added with 0.1 phr stabilizer and blended for a predetermined time of 3 min, which was recorded as the reaction time. Throughout the experiment, the temperature was maintained at 300 °C. The physical blend of pure PA66 and PEI was also prepared using the same procedure. The test specimens of PA/PEI and PA/fPEI blends were compression molded in an electrically heated hydraulic press. Hot-press procedures involved preheating at 300 °C for 5 min, followed by compressing for 2 min at the same temperature, then water cooled to room temperature for about 1 h. Note the weight ratio of PA66/PEI or fPEI was fixed at 60/40, which showed better processability and property improvement than other compositions.

Characterization

The nonisothermal degradation behavior of neat resins, fPEI, and their blends were characterized using a thermogravimetric analyzer (TGA Q500, TA Instrument). All measurements were performed under a nitrogen atmosphere in the temperature range between 30 and 800 °C at a heating rate of 10 °C min^{-1}.

Differential scanning calorimetry (DSC) was carried out under nitrogen flow at a heating rate of 10 °C/min using PerkinElmer DSC-7. A tiny as-extruded sample (ca. 10 mg) was used for DSC over a temperature range from 30 to 200 °C. Dynamic mechanical relaxation was measured with a Perkin Elmer model 7e DMTA working in bending mode constant stress. The complex modulus, $E* = E' + iE''$, of each sample was determined over a temperature range from 0 to 150 °C at a constant frequency of 1 Hz. The experiments were carried out at a heating rate of 10 °C/min. The dimension of the specimen samples was about $12 \times 12 \times 3$ mm. The specimen was cut from a core part of the injection-molded dumbbell specimen. Thermomechanical properties were measured on a thermomechanical analyzer (TA Model 2940). Size of the compression-molded

specimens was $7 \times 7 \times 3$ mm. The temperature range was from 30 to 140 °C and the heating rate was 5 °C/min. The expansion measurements used the flat-tipped standard expansion probe with a constant force of 0.05 N. All materials show temperature dependence in their linear coefficients of thermal expansion, CTE, especially above T_g (glass transition temperature). Therefore, a single reported number for CTE cannot accurately reflect the expansion behavior, except below T_g, where CTE changes little.

Infrared spectra were recorded on a Shimadzu FTIR spectrometer (Prestige-21) to identify the chemical groups of the reactive blends. The samples were measured in the form of thin film from compression molding. SEM images of the morphology of modified blends were observed by field-emission scanning electron microscope (FESEM) JSM-6400 (JEOL, Japan) with accelerating voltage at either 5 or 10 kV and working distance from 8.8 to 15.1 mm. The dispersed PEI/fPEI domain within the PA66 matrix was also observed. Both the freeze-fractured and the impact-fractured sample surfaces were sputter-coated with platinum using an ion coater IB-3 (Giko, Japan). Molau tests were performed by dissolving about 100 mg of the blend samples in 20 ml of 85 % formic acid, storing the test tubes for 24 h, and observing the turbidity of the solutions.

Notched Izod impact test was performed according to ASTM D256, using DG-1B (Toyo Seiki Co. Ltd.) after notching (sharp notches of 2.5 mm depth obtained with a diamond cutter). An average value of five replicated specimens was taken for each composition. Heat deflection temperature (HDT) was measured by an HDT tester, 6M-2 (Toyo Seiki Co. Ltd.) at edgewise mode under a load of 0.455 MPa at a heating rate of 2 °C/min according to ASTM D648. HDT was the temperature at which the specimen distortion increased to 0.25 mm during the heating process. Both impact and HDT tests were carried out for the as-mold samples. The melt flow index (MFI) measurements were performed at 300 °C on a GOTECH melt flow indexer Model 4002 according to ASTM D1238.

Results and discussion

IR spectroscopy results of PEI functionalization and interfacial reactions

IR spectroscopy was used to examine the structural changes in PEI following functionalization. Figure 1 shows the IR spectrum of the samples of neat PEI and fPEIs of PM10 (PEIgMA) and PG10 (PEIgGMA). The assignments of the principal absorption bands of PEI, 1780, 1720, due to symmetric and asymmetric stretching of C=O, respectively, and 1608 due to aromatic C=C, were made based on the literature [37, 38]. Some of these assignments are indicated in Fig. 1. In the spectrum of PM10, new absorption bands at 1700 and 1783 cm^{-1} due to symmetric stretching of carbonyl group of carboxyl acid and MA, respectively; and at 1854 cm^{-1} due to asymmetric stretching of MA, which are not observed in the spectrum of PEI, are found in the range 500–2500 cm^{-1} (line B). These characteristic bands are assigned to a carbonyl stretching in MA grafted on PEI. From these results, it is clear that MA units are introduced into the PEI backbone via
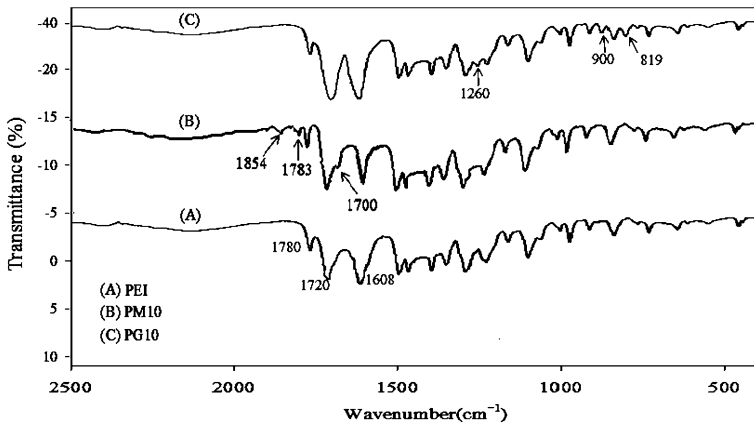
Fig. 1 FTIR spectra of *A* neat PEI, *B* PEI/MA10, and *C* PEI/GMA10

the reactive extrusion process. Line C is the FTIR spectrum of the GMA-grafted PEI (PG10). Compared with the spectrum of the neat PEI, we obtain a spectrum with a broadened signal in the region of 1720 cm^{-1} due to carbonyl stretching of both GMA and PEI. The C–O stretch is strong and appears as two bands, a broad band with a maximum near 1260 cm^{-1} (C–O stretching) and narrower and slightly weaker bands with maxima near 900 and 819 cm^{-1} (stretching of oxirane group). From these data, we conclude that the epoxy ring is grafted to PEI to a certain extent with the radical initiated reactions.

For investigating the reaction between PA66 and fPEI, the comparison of FTIR spectra of unmodified PA66/PEI and PA66/fPEI blends are shown in Fig. 2 together with neat PA66 and PEI. Figure 2a shows the range of 500–2000 cm^{-1}, and 2b in the range of 2000–4000 cm^{-1}. In Fig. 2a, the characteristic peaks of both neat PA66 and PEI can be observed clearly in the spectrum of unmodified PA66/PEI blend (Line b). The bands at 1635 and 1541 cm^{-1} are attributed to PA66 amide I and II absorption bands, respectively [39]. The principal absorption bands of PEI at 1780 and 1720 cm^{-1} also appear in PA66/PEI blends, but the band at 1608 cm^{-1} of PEI seems to merge with the band at 1635 cm^{-1} of PA66 and produces a broad band. Two new peaks appear in PA66/PM10 spectrum (line C) compared with that of unmodified PA66/PEI. The peak at 1854 cm^{-1} is assigned to the asymmetrical stretch vibrations of the anhydride carbonyl [40]. In addition, slightly broadened peak around 1705 cm^{-1} may result from the reaction between MA of PM10 and the end amino group of PA66 [41]. As for the spectrum of PA66/PG10, disappearance of epoxy ring band at 900 and 819 cm^{-1} in line D could illustrate that the reaction between two phases has occurred with epoxy ring. Since the spectrum of PA66/PG10 (line D) in the range of 500–2000 cm^{-1} is nearly the same as that of the PA66/PEI blend, we further examine the spectra in the range of 2000–4000 cm^{-1} in Fig. 2b. It can be clearly seen that the peak at 3305 cm^{-1} due to the N–H vibration is present in all spectra except neat PEI. In addition, in the spectrum of PA66/PG10 (line D), the OH stretching band at 3475 cm^{-1} is due to epoxy ring opening of GMA. The small shifts of N–H and OH band could stem from the H-bonding
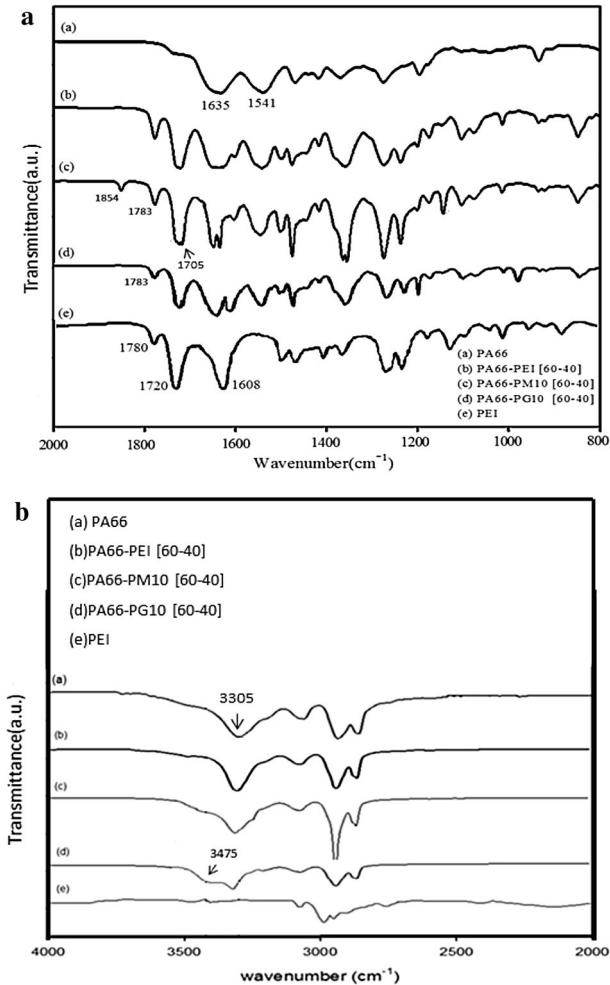
Fig. 2 **a** FTIR spectra for 500–2000 cm^{-1} of *a* neat PA66, *b* PA66/PEI, *c* PA66/PM10, *d* PA66/PG10, and *e* neatPEI. **b** FTIR spectra for 2000–4000 cm^{-1} of *a* neat PA66, *b* PA66/PEI, *c* PA66/PM10, *d* PA66/PG10, and *e* neatPEI

between N–H and OH [42]. The appearance of these characteristic peaks could reveal the reaction between PA66 and fPEI and producing PA66/fPEI copolymer at the interface of the blend. And as expected, the spectrum of PA66/PM10 seems nearly the same as that of unmodified PA66/PEI in the high energy range.

In summary, the thermal cleavage of DCP would yield radicals. It is speculated that the decomposed DCP free radicals may induce the hydrogen abstraction from the methylene groups of bisphenol A and initiate graft polymerization. The radicals may also react with the monomer to form a growing monomeric radical, whose radical character is able to be conveyed to the PEI backbone, and to induce MA or GMA graft copolymerization as well as homopolymerization [34]. As for the
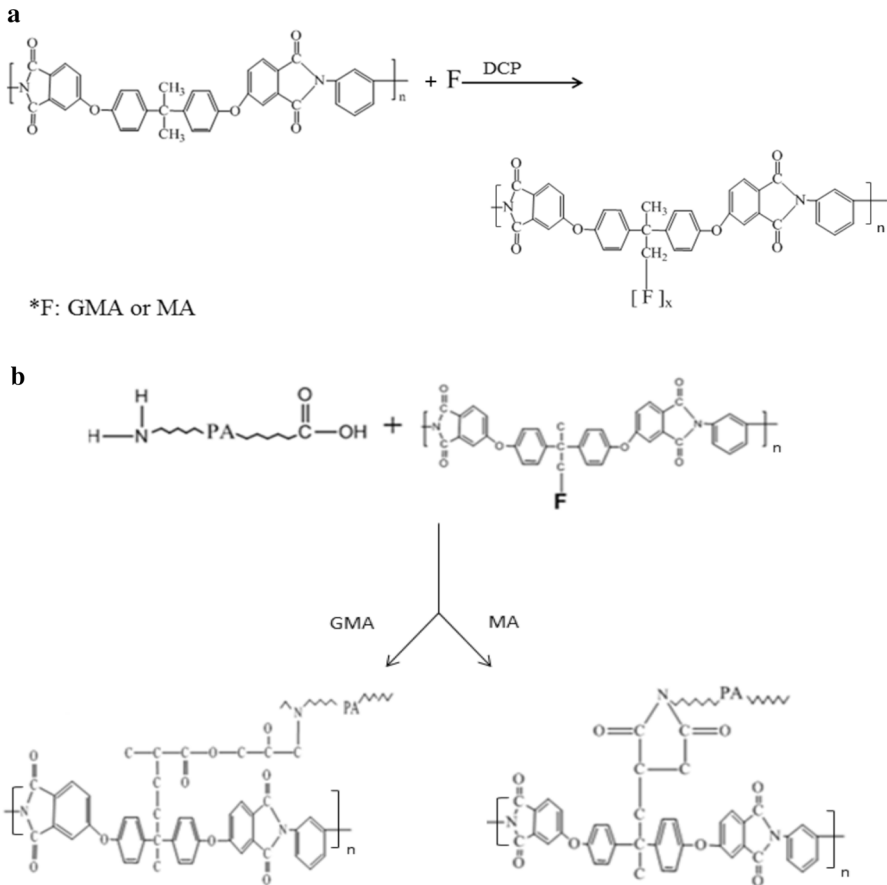
Fig. 3 **a** Scheme for PEI functionalization. **b** Scheme for interfacial reaction between fPEI and PA66

interfacial reaction between functionalized PEI and PA66, it has been demonstrated that either MA or GMA is highly reactive with the end-functional PA66 [40]. The reactions between functional group pairs, which are aliphatic amine/anhydride or epoxy, proceed extremely fast. According to the FTIR results, the schematics of PEI functionalization [34] and the interfacial reactions between fPEI and PA66 [43, 44] are shown in Fig. 3a, b, respectively.

Thermal and mechanical properties of functionalized PEIs

The thermal and mechanical properties of PEIgMA and PEIgGMA are listed in Table 2. It is apparent that all the measured properties are lower than that of neat PEI due to thermal hydrolysis and mechanical degradation experienced by fPEIs during compounding at 300 °C. It is obvious that PEIgMA suffered more loss in properties relative to PEIgGMA.

The addition of maleic anhydride may trigger the acid catalyzed degradation of PEI, which is similar to the degradation behavior of polyamide [45]. Indeed, we observed that PEIgMA darkened significantly after functionalization for a short compounding period of 5 min, with high degree of grafting (DG) PM10 appearing darker than low DG PM5. Further, while storage modulus exhibited significant decrease (ca. 50 % drop), T_g (from DMA), T_s (from TMA), and HDT (by ASTM D648) only showed mild loss against neat PEI. Note that the properties of high DG fPEIs also decreased more than that of low DG ones due to chain degradation induced by the presence of high content of reactive monomers.

Morphological study

Reduction of interfacial tension and increase in interfacial adhesion is the goal of compatibilization to achieve stable morphology in polymer blends [29, 30]. Figures 4 and 5 display the morphologies of the uncompatibilized and compatibilized blends before and after impact test observed by SEM. Figure 4 shows the micromorphologies of cryogenic fractured specimens of the uncompatibilized PA66/PEI blend (Fig. 4a), PA66/PM10 (Fig. 4b) and PA66/PG10 blends (Fig. 4c). All blends show binary phase structures with PEI dispersing in PA66 matrix, which are typical sea–island structures. However, the uncompatibilized blend gives a coarse morphology, in which aggregated or coalesced PEI droplets formed large particles with diameters of 1–2 μm. In addition, there are sharp interfaces between PEI particles and PA66 matrix with many voids of different sizes, indicating poor compatibility and low adhesion of the two phases [30]. As for the compatibilized blends (Fig. 4b, c), submicron fPEI droplets dispersed in PA66 matrix uniformly with diffused phase boundaries (see the edge of the droplets protruded from the fractured surface) can also be seen, indicating that the interfacial tension was reduced and the coalescence of the fPEI droplets was suppressed efficiently. Particularly, to show the interfacial interaction, a single large droplet, located at the center of Fig. 4b or c, is debonded from the matrix; however, the remaining shell-like, thickened interfacial regions [46, 47] can be clearly observed due to effective compatibilization.

To further demonstrate the effect of compatibilizer on the interfacial adhesion, SEM observation of impact-fractured section was also carried out. The SEM image of the uncompatibilized blend (Fig. 5a) shows rather smooth surface without the sign of plastic deformation of the matrix. It can be clearly seen that spherical PEI droplets debonded from PA66 matrix under impact, and the fractured surface is full of voids and large cracks. This is originated from the poor interfacial adhesion at the interface of the two phases in which the two components only exhibit partial miscibility. When the sample was subject to impact, PEI droplets debonded from PA66 matrix easily leading to the formation of voids. With increasing matrix deformation, the individual voids could coalesce together and finally cause the sample to break. In addition, the remaining droplets protruded from the surface show little shape change; and there are also some cracks along the phase boundaries with little fibrillation.

Fig. 4 SEM micrographs of cryo-fractured PA66/PEI and fPEI blends. **a** PA66/PEI blend. **b** PA66/PM10 blend. **c** PA66/PG10 blend
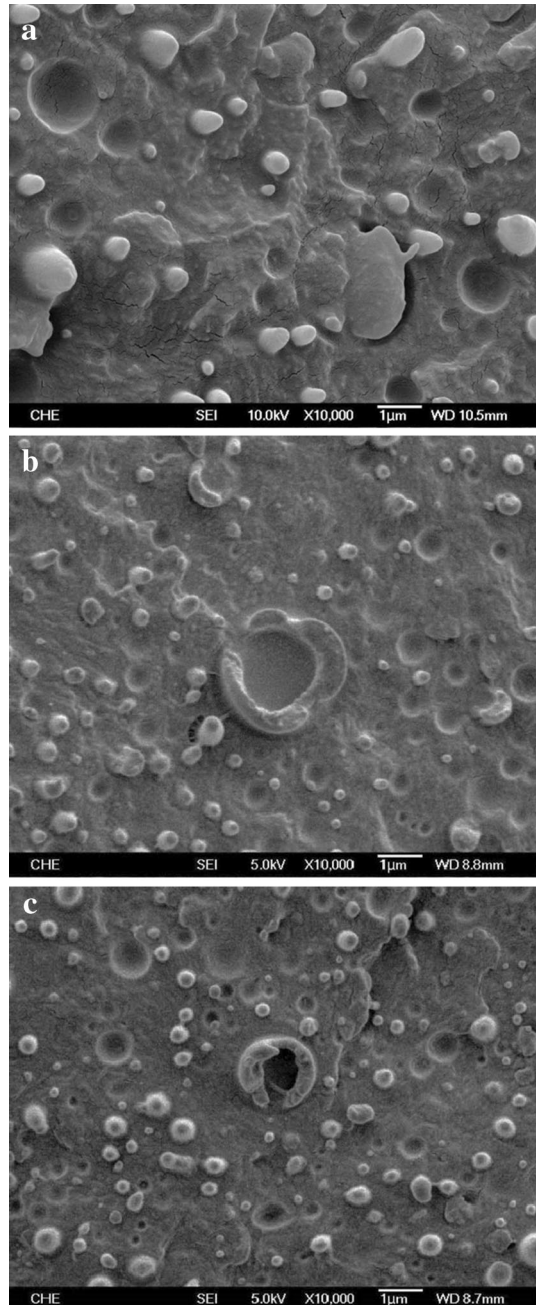
Different from that of the uncompatilized blend, most fPEI droplets did not debond from the matrix under impact for the compatibilized blend (Fig. 5b, c), and the originally spherical particles were elongated into elliptical ones during impact.
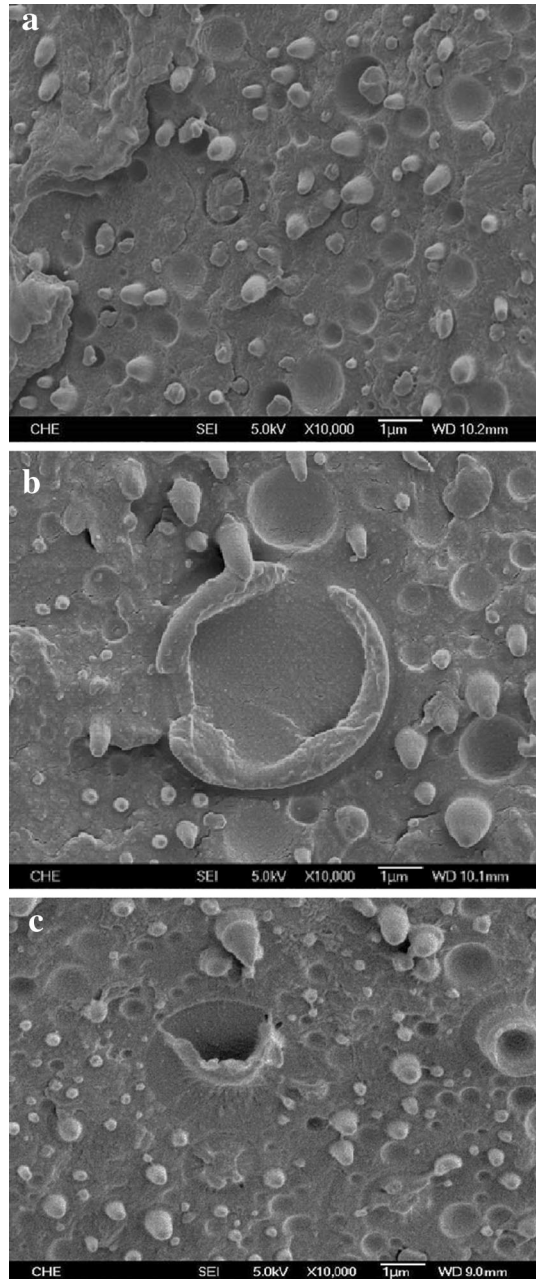
The particle distortion ratio, as defined by Kitayama et al. [48], could reach 3–5. Besides, no large cracks appear across the surface indicating that the fracture mode is changed from the debonding of PEI droplets to the failure of PA66 matrix by

blending with fPEI. Thus, the plastic deformation induced by the soft interface under external stress may lead to more anisometric droplets during the impact test for compatibilized blends. In short, the compatibility of the blend can be improved effectively by the addition of fPEI though two phases still exist in the blend. It is proposed that fPEI sits at the interface adhered to PA66 matrix by chemical bonding or chain entanglement with the two phases, which reduces the interfacial tension, suppresses coalescence of fPEI droplets, and also increases the interfacial adhesion. This mechanism of the compatibilization is further characterized by MFI and DMA tests.

Molau test

Molau test was used to analyze the emulsifying effect of a graft copolymer in the polyamide/polyolefin blends [16, 49]. Here, the observation of the solubility of each material helps us to predict and understand the interaction between each component in the blend. The Molau tests were carried out using formic acid as the solvent in transparent glass beakers for uncompatibilized PA66/PEI blend and compatibilized blend of PA66/PG10 (see Fig. 6). Formic acid is a good solvent for PA66 but a poor solvent for PEI, and vice versa for NMP. Indeed, PA66 is completely dissolved in formic acid and gives a transparent solution [4]. For the uncompatibilized PA66/PEI blend, PA66 can be dissolved completely in formic acid while leave the PEI particles floating upon the solution (Fig. 6a). After filtration, the vacuum dried PEI powder can also be dissolved in NMP and the solution is nearly transparent (Fig. 6b). It suggests that PA66 and PEI are almost incompatible and the interaction between them is weak. The compatibilized PA66/PG10 blend (Fig. 6c) exhibits an opaque suspension in the formic acid without apparently separated layer. Then after filtration, the vacuum dried powder, which consists of in situ-formed PA66/PG10 copolymer, cannot be completely dissolved in NMP showing an opaque suspension (Fig. 6d). This indicates that the addition of PEIgGMA no doubt increased the interaction between PA66 and PEI. It can serve as an emulsifying agent, and improve the compatibility of the two phases.

Thermal and degradation behavior of PA66/PEI Blends

Figure 7 shows the neat PA66 and the blend DSC thermograms of melting and cooling; and the characteristic parameters are listed in Table 3. From Fig. 6a, it can be seen that two melting peaks were present for neat PA66 and the PA66/PEI blend; they correspond to the melting of α (the major peak) and β (the minor peak) form crystals of PA66 [24]. However, the β peak was reduced to a shoulder for the PA66/fPEI blends due to the coupling reactions between PA66 and PEI. The melting peak temperatures, $T_m(\alpha)$, and the crystallizing peak temperature, T_c, showed no obvious change, while both the corrected ΔH_m and ΔH_c of PA66/fPEI blends increased a little in comparison with the neat PA66. The crystallization of polymers was controlled by nucleation and growth processes. On the one hand, the PEI droplets introduced could act as nucleating agents to increase the nucleation sites of the matrix; but the processing temperatures for PA66 and PEI were quite different and
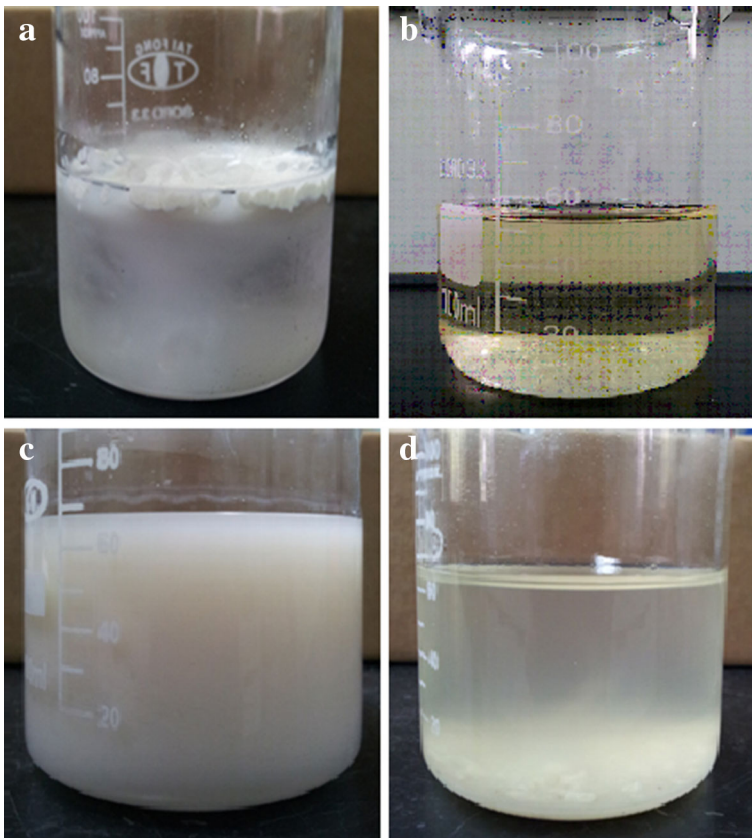
Fig. 6 **a** Uncompatiblized PA66/PEI blend in formic acid. **b** Dried filtrand dissolved in NMP. **c** Compatibilized PA66/PG10 blend in formic acid. **d** Dried filtrand dissolved in NMP

in the processing of the blends, and at the processing temperature, though was higher than the glass transition temperature of PEI, the PEI did not flow completely; so the interactions between PEI and PA66 would restrict the diffusion of the PA66 chain segments to the crystal surface and hinder the PA66 crystal growth in some degree. The consequence of the two opposite interactions was that the crystallinity of the blends increased slightly over that of neat PA66.

Figure 8 shows TGA thermograms (Fig. 8a) and their derivative weight curves (Fig. 8b). Only the measurements of modified blends of PA66/PG10 and PM10, along with neat PA66 and PEI, were presented for the reason of clarity. Thermal degradation profiles of the modified blends displayed that their stability was improved over the unmodified PA66/PEI blend. Furthermore, TGA thermograms for binary incompatible blends usually show two-step changes in weight loss with two distinct peaks corresponding to the degradation of each component in the DTG curves [50]. The specific interaction between polar amido and imide groups may improve the miscibility between PA66 and PEI phases, which result in only single-
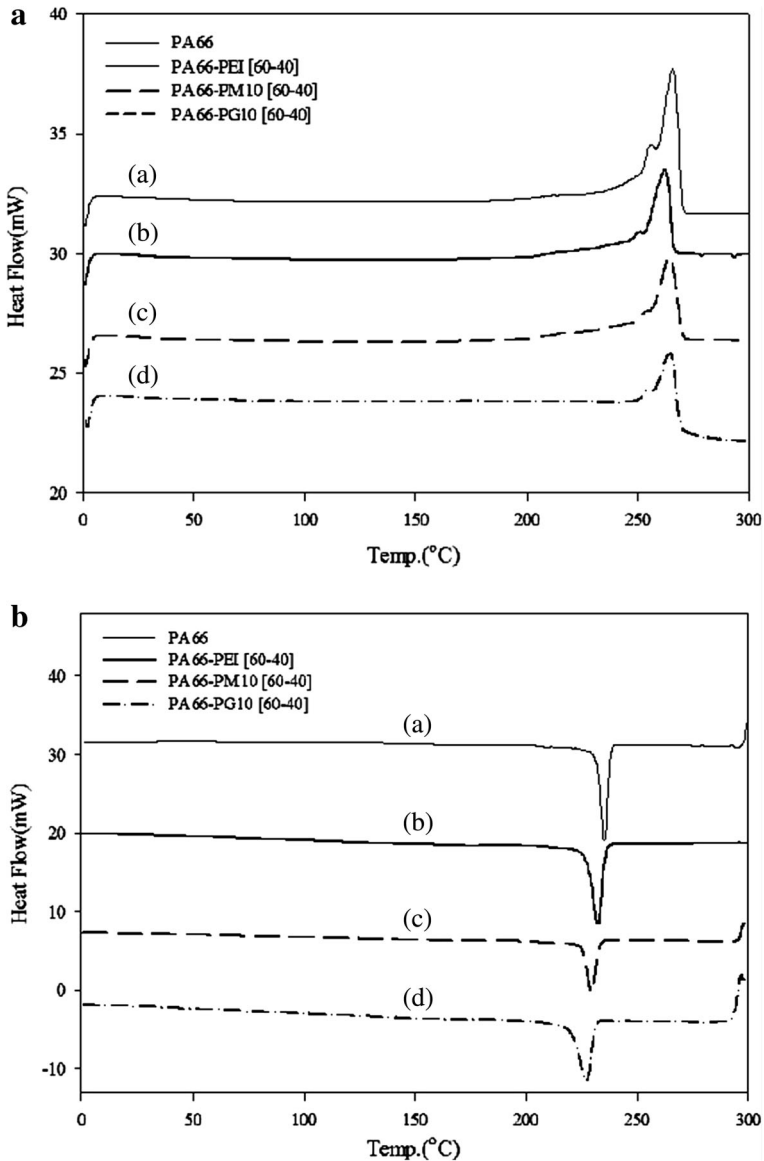
Fig. 7 DSC traces of *a* neat PA66, *b* PA66/PEI. *c* PA66/PM10, *d* PA66/PG10. **a** Heating scan; **b** cooling scan

step weight loss changes even in the unmodified blends. However, the unsymmetrical peaks in the DTG curves of various blends may represent overlapped stages of degradation [50, 51]. In addition, the shoulder in the DTG curves around 500 °C may imply some inhomogeneities in the phase-separated, unmodified blend as seen in Figs. 4 and 5. That the addition of fPEI makes the degradation peaks more symmetrical with a less clear shoulder may demonstrate the improvement in the

Table 3 Thermal and degradation properties of PA66/PEI and fPEI blends

Name code	T_m (°C)	ΔHc (J/g) corrected	T_c (°C)	ΔHc (J/g) corrected	T_d (°C)	RW (%)
PA66	265.7	57.7	235.7	52.3	460	3.2
PA66-PEI	264.2	62.2	232.3	64.2	446	9.0
PA66-PG5	265.5	59.7	229.2	63.2	457	10.6
PA66-PG10	266.3	56.3	227.4	55.7	452	9.1
PA66-PM5	267.2	66.2	230.6	65.5	455	9.5
PA66-PM10	265.8	61.5	229.2	64.8	450	9.3

morphological homogeneity due to enhanced interfacial interaction in the PA66/
fPEI blends. For the quantitative comparison of thermal stabilities among the tested
specimens, the maximum thermal degradation temperatures, T_d, evaluated from the
peak value of DTG curves are also summarized in Table 3, together with the
residual weight of each sample after degradation. It can be clearly seen that T_d of the
modified PA6/fPEI blends were all higher than the unmodified one, while the
residual weight of each blend almost unchanged. Further, T_ds of modified PA66/
PEIgMA blends were slightly higher than that of PEIgMA modified ones. Finally,
compared with the neat PA66, though the T_d became lower, the carbonaceous
residuals remained higher for the blend samples.

Melt flow index

Melt flow index (MFI) measurement has been utilized successfully to obtain
qualitative information concerning the chemical reaction in a reactively compat-
ibilized system [52]. The variation of MFI with fPEI of different degree of grafting
in the blend is shown in Table 4. Firstly, the values of MFI of all blends are between
that of PA66 (the highest MFI) and PEI (the lowest MFI). The MFI for the
uncompatibilized blend is 261 g, and the addition of fPEI can dramatically decrease
the MFI of the compatibilized blend. For low DG blends, the MFI of PA66/PG5 and
PM5 decreased to 250 and 253 g, respectively. For high DG blends, the MFI of
PA66/PG510 and PM10 decreased to 247 and 249 g, respectively. The decrease
should be attributed to the improved dispersion of fPEI particles in the matrix that
enhances the viscosity of the melt blend. Then, MFI of high DG blends generally
decreases more than that of low DG ones. It should be attributed to the reaction
between PA66 and PEIgGMA or PEIgMA results in high molecular weight
copolymers and increases the interfacial adhesion. The reaction between PA66 and
fPEI has also been confirmed by FTIR and SEM.

Dynamic mechanical thermal analysis

The investigation of dynamic relaxation behaviors in relation to the molecular or
segmental mobility are extensively used to elucidate the compatibility of blends.
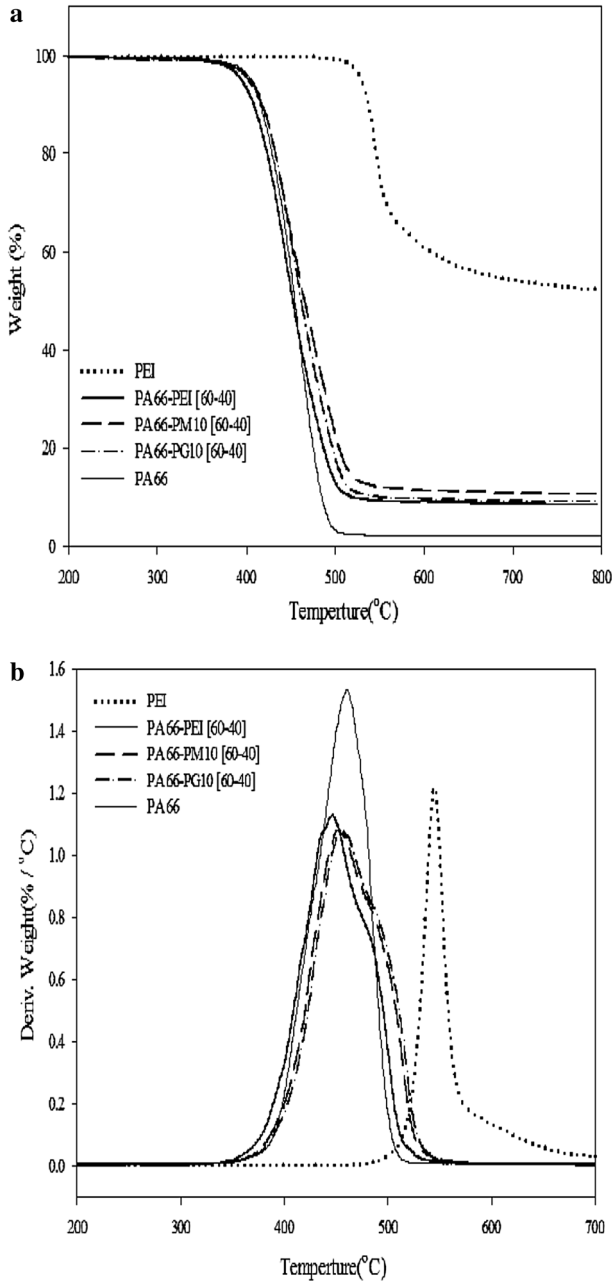Figure 9 shows plots of temperature dependence of storage (E') and loss (E″)

Fig. 8 a TGA thermograms and **b** DTG curves of neat resins and PA66/fPEI blends

moduli for neat PA66, PEI, uncompatibilized PA66/PEI and compatibilized PA66/fPEI blends. For the neat PA66, as shown in Fig. 9a, the E' curve shows typical behavior of a semicrystalline polymer with glass transition in the range of

Table 4 Thermal and mechanical properties of PA66/PEI and fPEI blends

Name code	T_g (°C)		E' (MPa)		T_s (°C)	MFI at 300 °C	HDT (°C)	IS (J/m)
			30 °C	200 °C				
PA66	74		514	97	212	270 ± 4.6	248	51.8 ± 2.3
PA66-PEI	63.8	217.2	382	122	212	261 ± 3.8	209	41.6 ± 1.5
PA66-PG5	74.6	215.7	448	178	217	250 ± 2.6	220	45.6 ± 0.8
PA66-PG10	81.7	216.5	412	155	220	247 ± 2.1	227	46.7 ± 0.8
PA66-PM5	68.6	214.4	443	179	219	253 ± 1.2	224	45.2 ± 1.1
PA66-PM10	72.0	216.6	352	143	214	249 ± 3.7	220	44.7 ± 0.7

50–100 °C; and a secondary transition due to crystalline domain slip around 160 °C. E' only slightly decreases before melting at 265.7 °C (from DSC) which is beyond the experimental temperature range shown here. On the other hand, for the neat PEI, the E' curve shows typical behavior of an amorphous polymer. E' remains nearly unchanged up to the glass transition around 220 °C. Note that the glassy E' of PA66 even higher than that of PEI. For PA66/PEI blends, both the glass transitions of PA66 and PEI domains are clearly broadened compared with that of neat resins. The E's of the PA66/fPEI blends are clearly greater than that of unmodified PA66/PEI; and E' of PA66/PG10 is even greater than that of PA66/PM10. The proton-catalyzed degradation of PM10 during high-temperature functionalization (see Table 2) due to the presence of MA moiety may lead to the low E' of PA66/PM10 blend. According to the characteristic changes of E', the E'' curve of neat PA66 shows the T_g (α-transition) at 76 °C; a shoulder around 160 °C; and a melting peak above 250 °C. For neat PEI, there is T_g (α-transition) at 223 °C with a broad β-transition around 132 °C [24]. The two peaks for Tgs of both PA66 and PEI domains apparently broadened in the blend samples; and the difference between T_gs of PA66 and PEI is the largest for unmodified PA66/PEI blend, and is the smallest for PA66/PG10 blend. These results indicate that the grafting of either MA or GMA functional group to PEI backbone improve the interfacial interaction of the PA66/PEI blend. For quantitative comparison, the T_gs and the E' values at 30 and 200 °C are listed in Table 4.

Thermal–mechanical behavior

The thermal–mechanical analysis is useful in studying the thermal expansion behavior of polymers. The dimensional changes vs temperature curves of the binary blends along with the neat PA66 and PEI resins are shown in Fig. 10a. The slope of the relative dimensional change, which is the linear coefficient of thermal expansion (CTE), of the specimens, is plotted in Fig. 10b against temperature. For neat PA66, the expansion increased with temperature, which is typical of semicrystalline polymers. PA66 retained its stiffness even above T_g (ca. 76 °C) as can be seen from DMA (Fig. 9a) in which E' remained flat before melting. In Fig. 10b, the CTE of PA66 showed a broad peak around 76 °C, indicating the glass transition. For neat
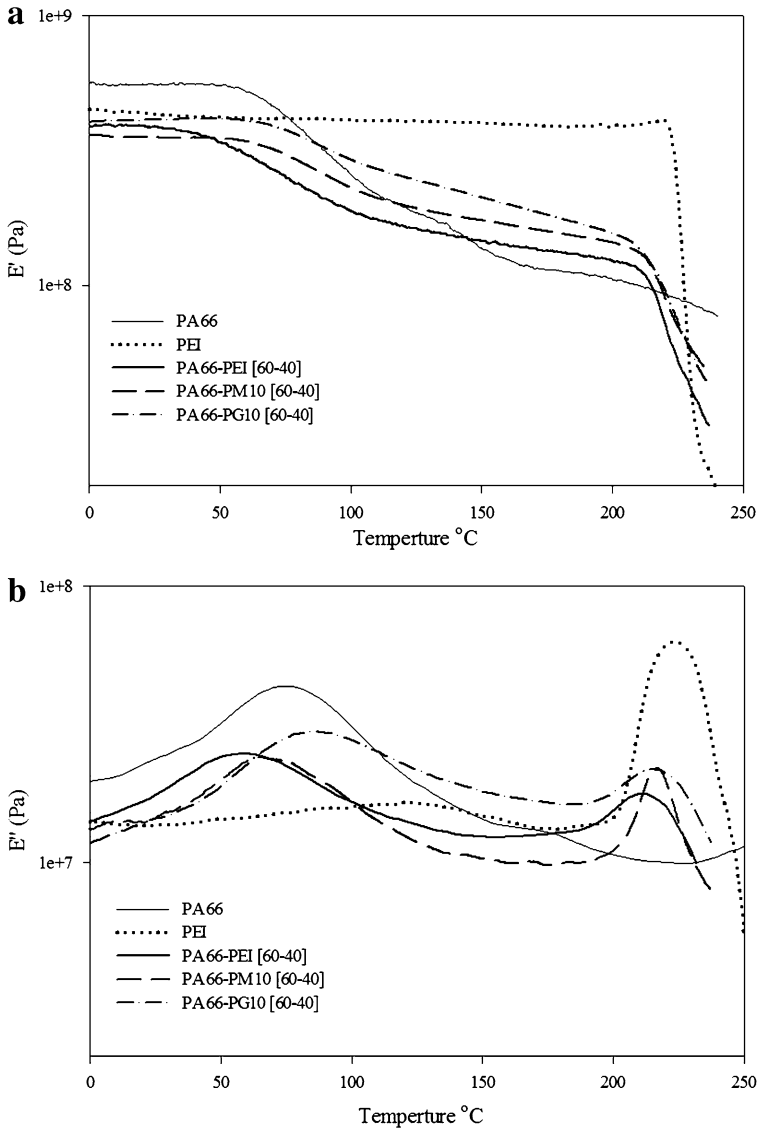
Fig. 9 DMA curves of storage and loss moduli of PA66/fPEI blends. **a** Storage moduli (E'); **b** loss moduli (E'')

PEI, there was little expansion before T_g (ca. 223 °C), and showed a step change in the specimen dimension passing the glass transition, which is typical of glassy polymers. As expected, a sharp peak in CTE of PEI can be seen in Fig. 10b corresponding to the E'' peak from DMA (Fig. 9b). Again in Fig. 10a, the unmodified PA66/PEI showed abrupt increase in thermal expansion after 150 °C, and a step change passing the T_g of PEI. For the modified blends of PA66/fPEI, the thermal expansion, which was clearly lower than that of uncompatibilized pair after
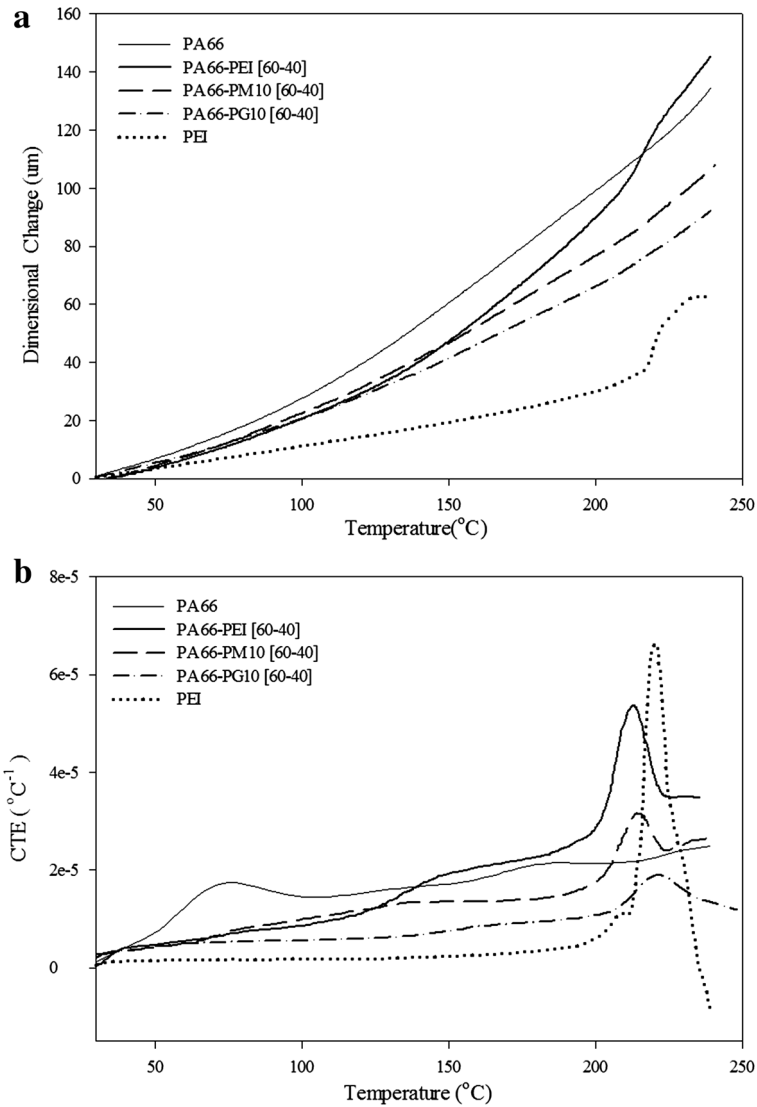
Fig. 10 TMA scans of neat resins and PA66/PEI blends. **a** Dimensional change vs temperature; **b** CTE vs temperature

150 °C, increased steadily until the T_g of PEI. The thermal expansion of the PA66/PG10 is the lowest among the tested blends. In Fig. 10b, the broad peak seen in the CTE of neat PA66 disappeared in the blends due to interaction with PEI. The CTE of all the blends showed a hump around 150 °C possibly due to softening of the interfaces (small shoulder in E'' around 150 °C). The peak around 220 °C for PEI glass transition broadened significantly for PA66/fPEI blends. Overall, the CTE of unmodified blend is the highest, and that of PA66/PG10 is the lowest among all the blends due to the enhanced interfacial adhesion. In addition, we also note that the

softening point Ts of PA66 at 212 °C due to melting of crystalline phase is lower than that of the modified PA66/fPEI blends.

Heat deflection temperature and impact property

The measurement of HDT is shown in Fig. 11, where the dimensional change is plotted against temperature. The HDT is defined as the temperature at which the dimensional change reaches 0.25 mm. The negative dimensional change indicates the initial expansion of the tested specimens. The neat PEI showed an HDT at 209 °C which is lower than its T_g at 223 °C (Table 1). However, the HDT of PA66 at 248 °C is much higher than its T_g at 76 °C (Table 1). In fact, the HDT of semicrystalline PA66 depends on many factors, such as crystallinity and thermal history, and it takes great caution in preparing the sample for HDT test. Further understanding of the HDT is possible through a direct correlation with the modulus–temperature behavior. For PA66, the storage modulus E' only drops moderately through the glass transition zone, and exhibits a "plateau" region between the glass transition and the melting transition (see E' curve in Fig. 9a). Hence, considerable stiffness is still retained even upon exceeding the HDT [53], which is responsible for the high HDT of PA66. For quantitative comparison, the measured HDTs are shown in Table 4 together with Izod impact strength (IS). The HDT of unmodified blend is 209 °C, which is the same as neat PEI, indicating weak interfacial interaction between PA66 and PEI. The HDTs of the modified blends (PA66/fPEI) are all higher than that of unmodified PA66/PEI. Among them, PA66/PG10 shows the highest HDT at 227 °C, which is ca. 20 % increase relative to that of the unmodified pairs. Moreover, note that high DG of PEIgGMA showed higher HDT than its low DG counterpart due to improved interfacial interaction. However, high DG of
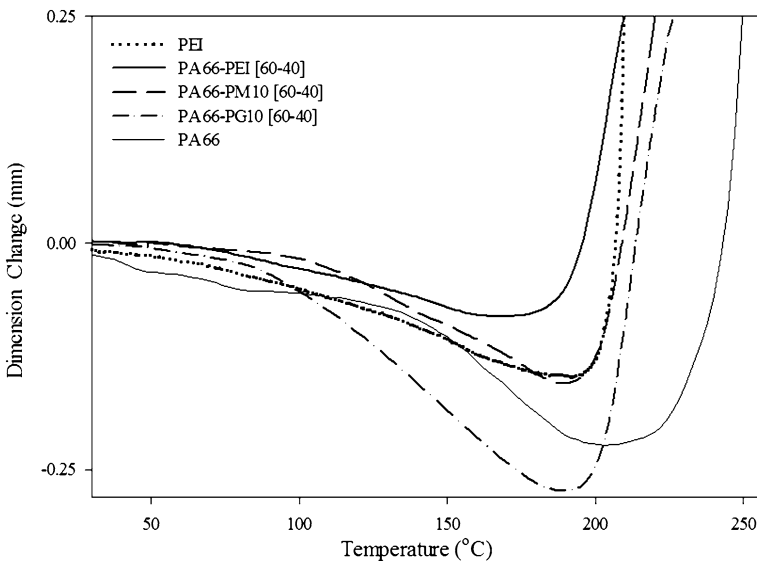

Fig. 11 HDT scans of neat resins and PA66/fPEI blends: dimensional change vs temperature

PEIgMA showed lower HDT than its low DG counterpart, since PEIgMA may suffer catalyzed oxidative degradation during high temperature compounding at 300 °C in the presence of excessive amount of MA. As can be seen from Table 2, high DG PM10 showed that the thermal and mechanical properties are the lowest among the functionalized PEIs.

Next, the increase in Izod impact strength can also be observed as a result of the improved compatibility. The IS of modified blends were generally greater than that of unmodified blend. Notably, the IS increased from 41.6 J/m of PA66/PEI to around 45 J/m of PA66/fPEI, which was ca. 10 % higher than that of unmodified blends. In fact, the fracture behavior changed from brittle to ductile with addition of fPEIs, as seen from SEM micrographs of the impact-fractured surfaces. Note that both IS and HDT of the modified PA66/fPEI blends were still lower than the neat PA66 except the high-temperature storage modulus; further refinement of DG and formulation will be required in the future research.

Conclusion

Novel PA66/fPEI blends based on functionalized polyetherimides were prepared successfully through melt compounding. fPEI promotes the compatibility of PA66/PEI blend and enhances the interfacial adhesion greatly by grafting PA66 through its amino end groups. SEM micrographs revealed sea–island morphology for the all binary blends. Ductile interfacial region between PA66 and fPEI domains on the impact-fractured surface can be seen as microfibrils at the domain boundaries indicating the compatibilizing effect of fPEI. In addition, fPEI droplets can disperse homogeneously in the PA66 matrix. Significant reduction of the size of spherical droplets of fPEI in the PA66 matrix further proves that the in situ-formed PA66-g-fPEI copolymer anchoring at the interface not only effectively reduces the interfacial tension, but also increases the interfacial adhesion.

As for the thermal and mechanical properties, the unmodified pairs showed typical low IS and low HDT of immiscible blend due to poor interfacial strength. However, the higher IS and HDT of PA66/PEIgGMA than that of PA66/PEIgMA may be attributed to the acid-catalyzed degradation of PEIgMA during compounding in the presence of MA monomer. The differences in glass transitions between fPEI and PA66 are much smaller than the unmodified blend. The T_g difference further reduced with high degree of grafting in both PEIgGMA and PEIgMA. Further, PEIgGMA with high DG (2.3 %) showed significant improvement in both IS and HDT of PA66 blend than low DG (1.9 %) one. On the contrary, PEIgMA with high DG (3.5 %) showed lower IS and HDT of PA66 blend than the low DG (2.4 %). While high degree of grafting promotes interfacial interaction, the high MA moiety seemed to harm the thermal and mechanical properties of PEIgMA leading to blends with poorer properties.

Finally, the proper formulation of the PA66/fPEI blends may optimize the advantages and eliminate some of the disadvantages associated with the functionalized PEIs. An optimized formulation may facilitate both toughness and heat resistance for PA66 blends. Further refinement of the blend formulation and blending conditions will be pursued in the future to take full advantage of the compatibilized blends.

References

 1. Paul DR, Bucknall CB (2000) Polymer blends: formulation and performance. Wiley, New York
 2. Utracki LA (1988) Commercial polymer blends. Chapman and Hall, London
 3. Utracki LA, Wilkie C (eds) (2014) Polymer blends handbook, 2nd edn. Springer, Berlin
 4. Kohan MI (1995) Nylon plastics handbook. Hanser Publishers, Berlin
 5. Shen L, Phang IY, Chen L, Liu T, Zeng K (2004) Nanoindentation and morphological studies on nylon 66 nanocomposites. I. Effect of clay loading. Polymer 45:3341
 6. Chen ZB, Li TS, Yang YL, Zhang Y, Lai SQ (2004) The effect of phase structure on the tribological properties of PA66/HDPE blends. Macromol Mater Eng 289:662
 7. Chang L, Zhang Z, Zhang H, Schlarb AK (2006) On the sliding wear of nanoparticle filled polyamide 66 composites. Compos Sci Technol 66:3188
 8. Harmia T, Friedrich K (1995) Mechanical and thermomechanical properties of discontinuous long glass-fiber-reinforced PA66/PP blends. Plast Rubber Compos 23:63
 9. Muratoglu OK, Argon AS, Cohen RE (1995) Microstructural process of fracture of rubber modified polyamides. Polymer 36:4771
10. Thomason JL (2007) Structure–property relationships in glass-reinforced polyamide. Part 3: effects of hydrolysis ageing on the dimensional stability and performance of short glass-fiber-reinforced polyamide 66. Polym Compos 28:344
11. Flexman EA Jr (1979) Impact behavior of nylon-66 compositions: ductile–brittle transitions. Polym Eng Sci 19:564
12. Liu X-Q, Zhan K-J, Wu X-J, Bao R-Y, Yang W, Yang M-B (2010) Studies on the blends of polyamide 66 and thermoplastic polyimide. J Macro Sci B 49:629
13. Rajatendu S, Sabharwal S, Bhowmick AK, Chaki TK (2006) Thermogravimetric studies on polyamide-6,6 modified by electron beam irradiation and by nanofillers. Polym Degrad Stab 91:1311
14. Wang HL, Shi TJ, Yang SZ (2006) Crystallization behavior of PA66/SiO2 organic–inorganic hybrid material. J Appl Polym Sci 101:810
15. Steller R, Micewicz E, Meissner W (2006) Structure and properties of polyamides-epoxidized elastomers blends. J Appl Polym Sci 99:1872
16. Zhang RC, Min M, Gao Y (2008) Nonisothermal crystallization of polyamide 66/poly (phenylene sulfide) blends. J Appl Polym Sci 107:2600
17. Weber M, Heckmann W (1998) Compatibilization of polysulfone/polyamide-blends by reactive polysulfones-evidence for copolymer formation. Polym Bull 40:227
18. Wang H, Lee KW, Chung T-S, Jaffe M (2000) Rheology, morphology and properties of LCP/Nylon 66 composite fibers. Polym Compos 21:114
19. Dawkins BG, Qin F, Gruender M, Copeland GS (2014) Polybenzimidazole (PBI) high temperature polymers and blends. In: DeMeuse MT (ed) High temperature polymer blends. Woodhead Publishing Ltd., Cambridge
20. Garcia JM, Garcia FC, Serna F, de la Pena JL (2010) High-performance aromatic polyamides. Prog Polym Sci 35:623
21. Robertson GP, Guiver MD, Yoshikawa M, Brownstein S (2004) Structural determination of Torlon® 4000T polyamide–imide by NMR spectroscopy. Polymer 45:1111
22. Long ER Jr, Collins WD (1988) The effects of fluids in the aircraft environment on a polyetherimide. Polym Eng Sci 28:823
23. Philipp HR, Le Grand DG, Cole HS, Liu YS (1989) The optical properties of a polyetherimide. Polym Eng Sci 29:1574
24. Sanchis MJ, Dıaz-Calleja R, Jaımes C, Belana J, Canadas JC, Diego JA, Mudarra M, Sellarès J (2004) A relaxational and conductive study on two poly(ether imide)s. Polym Int 53:1368
25. White SA, Weissman SR, Kambour RP (1982) Resistance of a polyetherimide to environmental stress crazing and cracking. J Appl Polym Sci 27:2675
26. Martinez JM, Equiazabal JI, Nazabal J (1993) Miscibility of poly(ether imide) and poly(ethylene terephthalate). J Appl Polym Sci 48:935
27. Chun YS, Lee HS, Kim WW (1996) Thermal properties and morphology of blends of poly(ether imide) and polycarbonate. Polym Eng Sci 36:2694

28. Chen H-L, Hwang JC, Chen C-C, Wang R-C, Fang D-M, Tsai M-J (1997) Phase behaviour of amorphous and semicrystalline blends of poly(butylene terephthalate) and poly(ether imide). Polymer 38:2747
29. Fayt R, Jerome R, Teyssie Ph (1986) Molecular design of multicomponent polymer systems, 13. Control of the morphology of polyethylene/polystyrene blends by block copolymers. Makromol Chem 187:837
30. Brown HR (2000) Strengthening polymer–polymer interfaces. In: Paul DR, Bucknall CB (eds) Polymer blends. Wiley, New York
31. Liu NC, Baker WE (1992) Reactive polymers for blend compatibilization. Adv Polym Technol 11:249
32. Xanthos M (1988) Interfacial agents for multiphase polymer systems: recent advances. Polym Eng Sci 28:1392
33. Xanthos M, Dagli SS (1991) Compatibilization of polymer blends by reactive processing. Polym Eng Sci 31:929
34. Shi Q, Su Y, Ning X, Chen W, Peng J, Jiang Z (2010) Graft polymerization of methacrylic acid onto polyethersulfone for potential pH-responsive membrane materials. J Membr Sci 347:62
35. He Z, Wang Y, Zhao T, Yeb Z, Huang H (2014) Ultrasonication-assisted rapid determination of epoxide values in polymer mixtures containing epoxy resin. Anal Methods 6:4257
36. Wang Y, Lin C-S (2014) Preparation and characterization of maleated polylactide-functionalized graphite oxide nanocomposites. J Polym Res 21:334
37. Smaoui H, Mzabi N, Guermazi H, Mlik Y, Agnel S, Toureille A, Schue F (2007) Characterisation of gamma-irradiated polyetherimide films with infrared spectroscopy and thermally stimulated current measurements. Polym Int 56:325
38. Silverstein RM, Webster FX, Kiemle D, Bryce DL (2014) Spectrometric identification of organic compounds, 8th edn. Wiley, NY
39. Herrero M, Benito P, Labajos FM, Rives V, Zhu YD, Allen GC, Adams JM (2010) Structural characterization and thermal properties of polyamide 6.6/Mg, Al/adipate-LDH nanocomposites obtained by solid state polymerization. J Solid State Chem 183:1645
40. Scott C, Macosko CW (1994) Model experiments for the interfacial reaction between polymers during reactive polymer blending. J Polym Sci B: Polym Phys 32:205
41. Yang H, Cao X, Ma Y, An J, Ke Y, Liu X, Wang F (2012) Effect of maleic anhydride grafted polybutadiene on the compatibility of polyamide 66/acrylonitrile–butadiene–styrene copolymer blend. Polym Eng Sci 52:481
42. Harani H, Fellahi S, Bakar M (1999) Toughening of epoxy resin using hydroxyl-terminated polyesters. J Appl Polym Sci 71:29
43. Orr CA, Cernohous JJ, Guegan P, Hirao A, Jeon HK, Macosko CW (2001) Homogeneous reactive coupling of terminally functional polymers. Polymer 42:8171
44. Macosko CW, Jeon HK, Hoye TR (2005) Reactions at polymer–polymer interfaces for blend compatibilization. Prog Polym Sci 30:939
45. Davis RD, Gilman JW, VanderHart DL (2003) Processing degradation of polyamide 6/montmorillonite clay nanocomposites and clay organic modifier. Polym Degrad Stab 79:111
46. Chang FC (1996) Compatibilized thermoplastic blends, Ch. 21. In: Olabisi O (ed) Handbook of thermoplastics. Marcel Dekker, New York
47. DeLeo CL, Velankar SS (2008) Morphology and rheology of compatibilized polymer blends: diblock compatibilizers vs crosslinked reactive compatibilizers. J Rheol 52:1385–1404
48. Kitayama N, Keskkula H, Paul DR (2001) Reactive compatibilization of nylon 6/styrene–acrylonitrile copolymer blends: part 3. Tensile stress–strain behavior. Polymer 42:3751
49. Molau GE (1965) Heterogeneous polymer systems: II. Mechanisms of stabilization of polymeric oil-in-oil emulsions. J Polym Sci A: Gen Pap 3:4235
50. Cock F, Cuadri AA, García-Morales M, Partal P (2013) Thermal, rheological and microstructural characterization of commercial biodegradable polyesters. Polym Test 32:716–723
51. Roeder J, Oliveira RVB, Becker D, Goncalves MW, Soldi V, Pires ATN (2005) Compatibility effect on the thermal degradation behaviour of polypropylene blends with polyamide 6, ethylene propylene diene copolymer and polyurethane. Polym Degrad Stab 90:481–487
52. Zhao R, Macosko CW (2002) Slip at polymer–polymer interfaces: rheological measurements on coextruded multilayers. J Rheol 46:145
53. Takemori MT (1979) Towards an understanding of the heat distortion temperature of thermoplastics. Polym Eng Sci 19:1104